Growth of n-type γ-CuCl with improved carrier concentration by pulsed dc sputtering: structural, electronic and UV emission properties

K. V. Rajani [1*], F. Olabanji Lucas [2], S. Daniels [1], D. Danieluk [3], A. L. Bradley [3], A. Cowley [2], M. M. Alam [2] and P. J. McNally [2]

[1]*Nanomaterials Processing Laboratory, NCPST, School of Electronic Engineering, Dublin City University, Dublin 9, Ireland*

[2]*Nanomaterials Processing Laboratory, The Rince Institute, School of Electronic Engineering, Dublin City University, Dublin 9, Ireland.*

[3]*Semiconductor Photonics Group, Physics Department, Trinity College Dublin, Dublin 2, Ireland*

* Corresponding author: Tel.: +353 1 700 5872, fax: +353 1 700 5508

Email Address: kv.rajani2@mail.dcu.ie

Abstract

γ Copper (I) chloride is naturally a direct band gap, zincblende and p-type semiconductor material with much potential in linear and non-linear optical applications owing to its large free excitonic binding energy. In order to fabricate an efficient electrically pumped emitter, a combination of both p-type and n-type semiconductor materials will be required. In this study, we report on the growth of n-type γ-CuCl with improved carrier concentration by pulsed dc magnetron sputtering of CuCl/Zn target. An improvement of carrier concentration up to an order of ~ 9.8×10^{18} cm^{-3}, which is much higher than the previously reported (~ 10^{16} cm^{-3}), has been achieved. An enhancement in crystallinity of CuCl along the (111) orientation and its consistency with the morphological studies have also been investigated as an effect of doping. Influence of Zn wt % in the sputtering target on the Hall mobility and resistivity of the doped films is explored. The strong ultraviolet emission of doped films is confirmed using room temperature and low temperature photoluminescence studies.

Keywords: n-Type CuCl thin films; sputtering; Photoluminescence; Semiconductor.

1. Introduction

The investigation of materials for solid-state lighting has a fundamental role in the development of cost-effective and environmentally friendly light sources. Wide band gap materials like GaN and ZnO are being studied extensively by many researchers for the past few years due to their potential applications in the fabrication of ultraviolet (UV) light emitting diodes (LEDs) and laser diodes [1-3]. But a crucial problem associated with these materials is the presence of threading dislocations due to the lattice mismatch with non-parental substrates [4, 5]. Furthermore, ZnO suffers from difficulties in producing consistent p-type material [6, 7]. The lattice mismatch between the semiconductor and the substrate can create defect densities as high as 10^{10} cm^{-2}. These defect densities tend to reduce the internal quantum efficiencies and hence the reliability of the devices [8]. The wide band gap, zincblende, I-VII compound semiconductor, γ-CuCl, could be a worthwhile candidate due to its small lattice mismatch with Si (<0.4 %), and it has a direct band gap of approx. 3.39eV at room temperature. Furthermore, the excitonic binding energy of CuCl is of the order of 190 meV [9], which is much higher than that of GaN (25 meV) [10], ZnO (60 meV) [11] and other related direct band gap inorganic materials. This exciton stability could see this material system develop into an efficient candidate for UV LEDs and diode lasers operable at room temperature. To make use of the advantages of CuCl in real devices, there should be a reliable technique for doping this material system.

There have been several reports on the electrical properties of cuprous chloride and related halides by many authors: Wagner *et al.* [12] studied the total electrical conductivity and hole conductivity of bulk copper halides (CuCl, CuBr and CuI) between 523 and 723 K using AC voltages at 1 kHz and DC polarization methods; Brendahan *et al.* [13] investigated the total conductivity and the electronic conductivity of CuBr thin films between 186 K and 350 K using impedance spectroscopy and DC polarization methods; Knauth *et al.* [14, 15]

performed room temperature Hall effect measurements and Mott-Schottky analysis on CuBr thick films, while Lucas *et al.* [16, 17] probed the total conductivity and the electronic conductivity of CuCl thin films between 160 and 400 K using impedance/admittance spectroscopy and DC polarization methods. The summary of all these experiments is that cuprous halides are naturally p-type mixed ionic–electronic semiconducting materials with a very low electronic conductivity at room temperature and above. The hole conductivity arises from a Cu deficiency δ, in the copper halide crystals ($Cu_{1-\delta}X$: where X = Cl, Br or I). As part of the effort for the realization of exciton related light emitting devices using CuCl, O'Reilly e*t al*. [18] co-evaporated CuCl/$ZnCl_2$ thin films and demonstrated the first n-type CuCl based films. However, the carrier concentration in these doped films was very low (n~ $1 \times 10^{16}/cm^3$) probably due to compensation effects caused by the simultaneous introduction of excessive Cl atoms from the co-evaporation of $ZnCl_2$.

Here, we proceed from our previous work on the growth and characterization of CuCl films [17-19] and move a step closer to the realization of an efficient homojunction light emitting device based on CuCl technology by presenting the optoelectronic properties of n-type CuCl:Zn thin films with improved carrier concentrations grown by pulsed dc magnetron sputtering on glass and Si substrates. Unlike the vacuum evaporation technique, sputtering is capable of depositing thin films of repeatable stoichiometry [20] which is crucial for the reliable performance of a compound semiconductor material like CuCl:Zn. In addition to this, the use of Zn powder instead of $ZnCl_2$ will prevent the problems of additional Cl inclusion during film deposition as was experienced in the co-evaporation of CuCl/$ZnCl_2$ films [18].

2. Experimental details

Thin films of CuCl:Zn were prepared by pulsed dc magnetron sputtering of a CuCl/Zn target, with the weight percentage of Zn in the target varying from 0-5%, onto glass and Si substrates. Prior to deposition the substrates were ultrasonically cleaned using acetone,

trychloroethane and methanol followed by de-ionised water. An ENI RPG-100 pulse generator was used to drive a planar magnetron fitted with the target in the power regulation mode. The chamber was first pumped down to a base pressure of $2x10^{-5}$ Pa by cryogenic pumping. The target was pre-sputtered for about 10 minutes prior to deposition in order to reduce the contamination and to obtain a stable plasma density. Sputtering was carried out in pure argon atmosphere and the working pressure was adjusted to 0.55 Pa. The target to substrate distance was adjusted to 6 cm. The power density at the target and duty cycle of the pulse were optimized from a number of iterations to be 1.73 W/cm^2 and 40%, respectively. The substrates were held at floating potential and the sputtering time was adjusted to 15 minutes to obtain a uniform film thickness of 350 ± 20 nm for all the deposited samples.

X-Ray diffraction (XRD) analysis was carried out using Copper K_α radiation of wavelength 1.54 Å from a Bruker D8 instrument to determine the crystallinity of the CuCl:Zn films, using θ–2θ configuration. The morphology of the thin films was investigated using Scanning Electron Microscopy (SEM) at an operating voltage of 13 kV. Circular gold ohmic contacts of 1mm diameter were evaporated on the films deposited on glass substrates. Hall effect measurements were carried out in the van der Pauw configuration using a Nanometrics HL5500PC Hall effect system. UV/Vis absorption spectra of the films were explored using a Perkin Elmer Lambda 40 UV/Vis spectrometer in a range of wavelengths from 320-420 nm. Temperature dependent photoluminescence (PL) measurements were carried out from room temperature down to 17 K by employing a closed helium cryostat system and a 355 nm excitation laser. The photoluminescence spectra were collected on a Jobin Yvon-Horiba Triax 190 spectrometer coupled with liquid nitrogen cooled CCD detector.

3. Results and discussion

The CuCl:Zn films (samples) are deposited on glass and Si (100) substrates at room temperature by pulsed dc magnetron sputtering of CuCl/Zn targets containing 0, 1, 3 and 5wt.

% Zn, and from here onwards these samples are designated as A, B, D and E, respectively (See Table 1). The crystalline quality of the CuCl:Zn films was examined and the corresponding diffraction peaks were indexed. In Figure 1(inset), plots (a), (b), (c) and (d) show the powder XRD pattern of samples A, B, D and E, respectively. All the measurements were carried out in identical experimental conditions. The Bragg diffraction patterns of the samples are in good agreement with the ICDD data for polycrystalline CuCl. All the samples show the cubic zincblende structure with lattice planes oriented along (111), (220) and (311) directions with 2θ values ~28.5°, ~47.4° and ~56.3°, respectively, and preferential orientation along the (111) planes. XRD patterns indicate no sign of structural deformity of CuCl by doping with Zn up to sample E; however, interestingly, an improvement in the orientation along the (111) direction is observed in samples B and D in comparison to that of sample A. The variation of the peak intensity ratio of CuCl (111) to the total intensity of all orientations {CuCl (111) + CuCl (220) + CuCl (311)} (between 2θ values 20^o and 60^o) as a function of the Zn wt. % is also illustrated in figure 1. One observes that the (111) crystalline volume fraction (crystallinity) increases with Zn doping up to sample D, and beyond that it tends to degrade. Generally, polycrystalline cuprous halide thin films are believed to contain numerous copper vacancies [21-23]. The introduction of Zn is assumed to fill some of the Cu vacancies in the CuCl crystal, thereby improving the crystallinity of the doped samples. The incorporation of Zn atoms could be facilitated due to the fact that the ionic radii of the Cu^+ and Zn^{2+} ions in the tetrahedral co-ordination are equivalent with a value of ~60 pm [24].

Figure 2 illustrates the variation of the full width at half maximum (FWHM) of the CuCl (111) peak and the average crystalline size in accordance with the weight percentage of Zn in the target obtained from the X-ray diffraction analysis. The average crystalline sizes are calculated using the Scherrer equation,

$$d = \frac{0.9\lambda}{\Delta\theta\cos\theta_B} \qquad (1)$$

where λ, θ_B and Δθ are the X-ray wavelength, Bragg diffraction angle and FWHM of the CuCl (111) peak corrected for instrumental broadening respectively. Since the lattice mismatch between the Si (a_{Si} =5.43 Å) and CuCl film (a_{CuCl} =5.40 Å) is very small (~0.5%), we expect that the broadening effect due to strain is negligible in this case. The FWHM decreases from 0.24^o (sample A) to 0.18^o (sample D) and again increases slightly to 0.2^o for sample E. This clearly indicates an improvement in the crystallinity of the CuCl film with the inclusion of Zn, and the maximum is achieved for the sample D. The average crystallite sizes of samples A, B, D and E are calculated as approx. 37 nm, 47 nm, 49 nm and 44 nm, respectively. The minimum FWHM and the maximum peak intensity ratio of the CuCl (111) with respect to all orientations are observed for sample D. Furthermore, the largest crystallite size is also noticed for the aforementioned sample. From the XRD results, one observes that the doping of CuCl films with 3 wt. % Zn (sample D) appears to be the optimum process and further increases in target Zn concentrations result in a reduction in the (111) crystalline volume fraction and crystalline size (sample E). The reduction in the crystal properties may be due to the segregation of dopants in the grain boundaries beyond a doping level corresponding to sample D (> 3 wt. % Zn in the target). This hypothesis is examined using SEM analysis of the appearance of non-uniform grains with irregular orientations.

SEM micrographs of the CuCl:Zn thin films are shown in figure 3, which indicates changes in the grain morphology as a function of Zn incorporation in the film. The images clearly show a slight increase in the grain size from samples A to D. The average crystalline sizes obtained from the SEM images are greater than those obtained from the Scherrer equation using XRD patterns. Similar results were reported by Natarajan *et al*. [19] in sputtered CuCl thin films using atomic force microscopy and XRD studies. The grains in the

SEM images can be considered as a group of aggregated nanocrystallites. The SEM images of samples A, B and D show almost homogeneous grain morphology, with uniform orientation of grains, while that of the sample E shows grains with irregular size and shape with different orientations. This is confirmed by the XRD pattern via a decrease in the peak intensity ratio of the CuCl (111) peak to total intensity of all orientations as shown in figure 1.

The room temperature Hall effect data for the Zn doped CuCl samples measured in the van der Pauw configuration are shown in figure 4. Hall measurements were not possible with the undoped CuCl (sample A), due to the high resisitivity of the sample. The presence of mixed conduction mechanisms was observed for sample B (1 wt. % Zn): both p-type and n-type conductivities with a relatively lower n-type carrier concentration of the order of ~ $10^{15}cm^{-3}$. This could be explained by dopant compensation via the simultaneous existence of both types of conductivity, i.e. electron conduction due to the inclusion of Zn in the Cu vacancies and hole conduction due to the well known naturally occurring Cu vacancies in the undoped CuCl. Due to the fluctuations in the data for the sample B, we included the results for an additional sample developed from a 2 wt. % Zn doped target (sample C) as well. The doped films (Zn wt. % > 1) consistently showed n-type conductivity with an increase of carrier concentration from 3.01±1.99 $x10^{16}$ cm^{-3} to 9.8±1.2 $x10^{18}$ cm^{-3} for samples C and D respectively, and then slightly decreases to 7.1±1.2 $x10^{18}$ cm^{-3} for sample E. The slight decrease in the carrier concentration of sample E with respect to sample D is assumed to be due to the fact that relatively fewer Zn atoms can contribute to the conduction, and instead can segregate to the grain boundaries beyond a particular concentration, in this situation corresponding to sample D (3 wt. % Zn). A similar reduction in carrier concentration of Al doped ZnO films were reported by Kim et al. [25]. As one expects, the Hall mobilities of the doped films were found to decrease as the Zn % increases. A mobility value of 20±8 $cm^2V^{-1}s^{-}$

[1], 0.1±0.02 $cm^2V^{-1}s^{-1}$ and 0.07±0.01 $cm^2V^{-1}s^{-1}$ was deduced for sample C, D, and E respectively. In a simple form, the Hall mobility may be expressed in terms of impurity scattering mobility μ_i and grain boundary scattering mobility μ_g as follows:

$$\frac{1}{\mu_h} = \frac{1}{\mu_i} + \frac{1}{\mu_g} \qquad (2)$$

The sharp decrease in the mobility from sample C (2 wt. %Zn) to D (3 wt. % Zn) can be attributed mainly to the impact of increased impurity scattering. The presence of grain boundaries and trapped interface charges in semiconductors results in inter-grain band bending and potential barriers which are well known to cause a considerable reduction in the resultant Hall mobility [26]. A further reduction in the mobility of sample E in comparison to sample D may be ascribed to be the combination of both impurity scattering and grain boundary scattering mechanisms as the presence of more grain boundaries was observed in the SEM image of sample E (see figure 3).

The variation of resistivities of the samples is also illustrated in figure 4 (inset). A value of 250 Ω cm was previously reported as the room temperature resistivity for undoped CuCl films using 4 point probe measurement [18]. The resistivities of the samples decrease to a minimum value of ~ 6 Ω cm for the sample D, and increase to ~ 11 Ω cm for sample E. Obviously, the reduction of resistivity of sample D is due to higher carrier concentration while the slight increase in resistivity of the sample E is due to a slight reduction in carrier concentration perhaps combined with the effect of increased grain boundary scattering as explained earlier. The electrical measurements confirm the efficacy of pulsed dc magnetron sputtering as a means of incorporating Zn in to the CuCl crystal lattice. The substitutional Zn leads to optimal carrier concentrations and resistivities for 3 wt. % Zn in the CuCl/Zn sputter target. We are currently looking at means of improving the mobility of these doped samples

via post deposition thermal treatments. In addition X-ray fine structure experiments are planned in order to confirm the substitutional site for Zn, i.e. Zn_{Cu}.

The room temperature UV-Vis absorption spectra for the CuCl:Zn films is shown in figure 5. Herein, the major peaks correspond to both high and low energy excitonic bands known as the $Z_{1,2}$ and Z_3 excitons, respectively. The $Z_{1,2}$ and Z_3 excitons are due to the coupling of the lowest conduction band state Γ_6 to both the uppermost valence band holes, Γ_8 ($Z_{1,2}$) and Γ_7 (Z_3), respectively [9, 27]. The $Z_{1,2}$ peak at ~ 372 nm (3.34eV) and the shoulder Z_3 peak at ~ 379 nm (3.28eV) are in good agreement with the previously reported absorption data for the undoped CuCl [18].

The PL measurements for all the samples (both doped and undoped) showed similar excitonic emissions at all temperatures. Figure 6 shows the temperature dependence of the PL spectrum of sample D. This graph clearly delineates four main peaks represented as Z_3 (~3.21eV), I_1 (~3.19eV), M (~3.17eV) and N_1 (~3.14eV), corresponding to the Z_3 free exciton, I_1 impurity bound exciton, M free biexciton and N_1 impurity bound exciton, respectively. The impurity corresponding to the I_1 peak has already been reported as being due to a copper vacancy [28], the M free biexciton results from exciton-exciton collisions [9] and the N_1 peak originates from a biexciton bound to an impurity. These results are in agreement with the previously reported low temperature PL data of the undoped CuCl [17, 18], indicating that the optical properties of the doped films are not compromised as a result of incorporation of Zn atoms. As the temperature increases, the rate of decrease of the peak intensities of I_1 and N_1 become higher compared to that of the Z_3 free excitonic peak intensity, and the spectra become dominated by the Z_3 peak above 100 K up to room temperature due to the high free excitonic binding energy of CuCl. The influence of temperature on the Z_3 free exciton peak is manifested as a peak energy shift from ~3.205 eV to ~3.248 eV for a temperature increase from 17 K to room temperature. The increase in the energy value of the

Z_3 free exciton as the temperature increases corresponds to an increase in the band gap energy and was theoretically and experimentally analysed for undoped CuCl samples by Garro *et al.* [29]. Analogous results in thin films and nanocrystals of CuCl have been reported previously [30, 31].

4. Conclusion

A reliable method for the development of n-type CuCl with improved carrier concentration using pulsed dc magnetron sputtering has been presented in this study. The resistivity of the Zn doped CuCl film was found to decrease by more than an order of magnitude compared to the undoped CuCl film with an average maximum carrier concentration of ~ 9.8×10^{18} cm^{-3} and a minimum average resistivity of ~ 6 Ωcm for 3 wt. % Zn doped samples. Improvement in the crystallinity of CuCl films by doping with Zn has been investigated, and maximum crystallinity is obtained for 3 wt. % Zn doped sample. The strong UV emission of the doped films confirms its utility in the optoelectronic field.

Acknowledgements

This project was funded by the Science Foundation Ireland Research Frontiers Programme (Project#06/RFP/ENE/027) and by the Enterprise Ireland Commercialisation Fund for Technology Development (Project# CFTD/07/IT/331). This work was part-funded by the Irish Higher Education Authority PRTLI "INSPIRE" project. The authors would like to thank Mr. Billy Roarty for his technical support.

References

[1] S. Nakamura, T. Mukai, T. Senoh, Appl. Phys. Lett. 64 (1994) 1687.

[2] Y. Ryu, T.S. Lee, J.A. Lubguban, H.W. White, B.J. Kim, Y.S. Park, C.J. Youn, Appl. Phys. Lett. 88 (2006) 241108.

[3] D.M. Bagnall, Y.F. Chen, Z. Zhu, T. Yao, S. Koyama, M.Y. Shen, T. Goto,

Appl. Phys. Lett. 70 (1997) 2230.

[4] J.K. Jeong, J.H. Choi, H.J. Kim, H.C. Seo, H.J. Kim, E. Yoon, C.S. Hwang, H.J. Kim, J. Cryst. Growth 276 (2005) 407.

[5] X. Li, S.G. Bishop, J.J. Coleman, Appl. Phys. Lett. 73 (1998) 1179**.**

[6] T.M. Barnes, K. Olson, C.A. Wolden, Appl.Phys.Lett. 86 (2005) 112112.

[7] K. Minegishi, Y. Koiwai, Y. Kikuchi, K. Yano, M. Kasuga, A. Shimizu, Jpn. J. Appl. Phys. 36 (1997) L1453.

[8] A. Bergh, G. Craford, A. Duggal, R. Haitz, Phys. Today 54 (2001) 42.

[9] M. Nakayama, H. Ichida, H. Nishimura, J. phys.: Condens. Matter 11(1999) 7653.

[10] B. Monemar, Phys. Rev. B. 10 (1974) 676.

[11] Y.R. Ryu, T.S. Lee, H.W. White, Appl. Phys. Lett. 83 (2003) 87.

[12] J.B. Wagner, C.Wagner, J. Chem. Phys. 26 (1957) 1597.

[13] M. Bendahan, C. Jacolin, P. Lauque, J.L. Seguin, P. Knauth, J. Phys. Chem. B 105 (2001) 8327.

[14] P. Knauth, Y. Massiani, J. Electroanal. Chem. 442 (1998) 229.

[15] P. Knauth, Y. Massiani, P. Pasquinelli, Phys. Stat. Sol. 165 (1998) 461.

[16] F.O. Lucas, P.J. McNally, S. Daniels, D.M. Taylor, J. Mater. Sci: Mater. Electron. 20 (2009) S144.

[17] F.O. Lucas, A. Mitra, P.J. McNally, S. Daniels, A.L. Bradley, D.M. Taylor, Y.Y. Proskuryakov, K. Durose, D.C. Cameron, J. Phys. D: Appl. Phys. 40 (2007) 3461.

[18] L.O'Reilly, A. Mitra, G. Natarajan, O.F. Lucas, P.J. McNally, S. Daniels, D.C. Camron, A.L. Bradley, A. Reader, J. Cryst. Growth 287 (2006) 139.

[19] Gomathi Natarajan, S. Daniels, D.C. Cameron, L.O'Reilly, A. Mitra, P.J. McNally, O.F. Lucas, R.T. Rajendra Kumar, I. Reid, A.L. Bradley, J. Appl. Phys.100 (2006) 033520.

[20] R. Schmidt, A. Basu, A.W. Brinkman, J. Eur. Ceram. Soc. 24 (2004) 1233.

[21] S. Kondo, K. Mikami, T. Saito, Opt. Mater. 30 (2008) 473.

[22] R.S. Bradley, D.C. Munro, P.N. Spencer, Trans. Faraday. Soc. 65 (1969) 1912.

[23] M. Ueta, H. Kazaki, K. Kobayashi, Y.Toyozawa, E. Hanamura, Excitonic Processes in solid (Springer : Berlin. 1986).

[24] R. D. Shannon, Acta Crystallogr. A 32 (1976) 751.

[25] K.H. Kim, K.C. Park, D. Y. Ma, J. Appl. Phys. 81(1997) 7764.

[26] T. Pisarkiewicz, K. Zakrzewska, E. Leja, Thin Solid Films 174 (1989) 217.

[27] A. Goldmann, Phys.Stat. Sol (b). 81 (1977) 9.

[28] M. Certier, C.Wecker, S. Nikitine, J. Phys. Chem. Solids 30 (1969) 2135.

[29] N. Garro, A. Cantarero, M. Cardona, T. Ruf, A. Gobel, C. Lin, K. Reimann, K. Rtibenacke, M. Steube, Solid State Commun. 98 (1996) 27.

[30] A.Gobel, T. Ruf, M. Cardona, C.T. Lin, J. Wrzesinski, M. Steube, K. Reimann, J.C. Merle, M. Joucla, Phys. Rev. B. 57 (1998) 15183.

[31] O. Pages, H. Erguig, A. Lazreg, A. Katty, A. Lusson, O. Gorochov, Mater. Sci. Eng. B 69 (2000) 431.

List of figure captions:

Figure 1. Variation of (111) peak intensity to the total intensity of all orientations as a function of the Zn wt. % in the target. The inset graph shows the X-Ray powder diffraction pattern for samples corresponding to (a) 0 wt. %, (b) 1 wt. %, (c) 5 wt. % and (d) 3 wt. % Zn doped CuCl targets.

Figure 2. Variation of FWHM of CuCl (111) peak and average crystal size of the CuCl: Zn film as a function of the weight percentage of Zn in the target.

Figure 3. SEM micrographs of CuCl: Zn films with (a) 0 wt. %, (b) 1 wt. %, (c) 3 wt. %, and (d) 5 wt. % Zn in the target.

Figure 4. Variation of resistivity, carrier concentration and mobility (inset) as a function of the wt. % of Zn in the target. Sample notation is indicated in Table 1.

Figure 5. Room temperature UV-Vis absorption of (a) 3 wt. % Zn doped CuCl and (b) undoped CuCl.

Figure 6. Temperature dependence and room temperature PL spectrum (inset) of 3 wt. % Zn doped CuCl films.

Table 1

Sample notation used in the text.

Sample	Wt % of Zn in the target
A	0
B	1
C	2
D	3
E	5

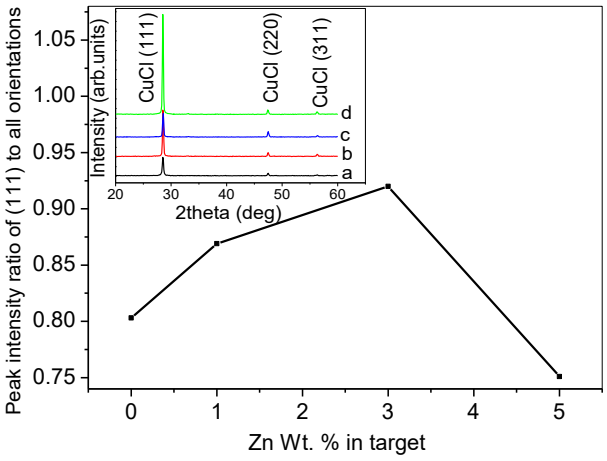

Figure 1

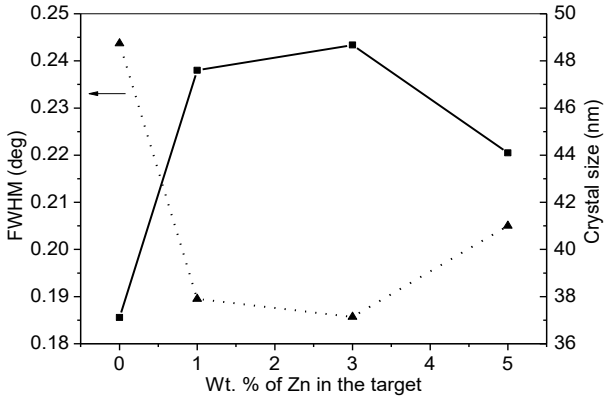

Figure 2

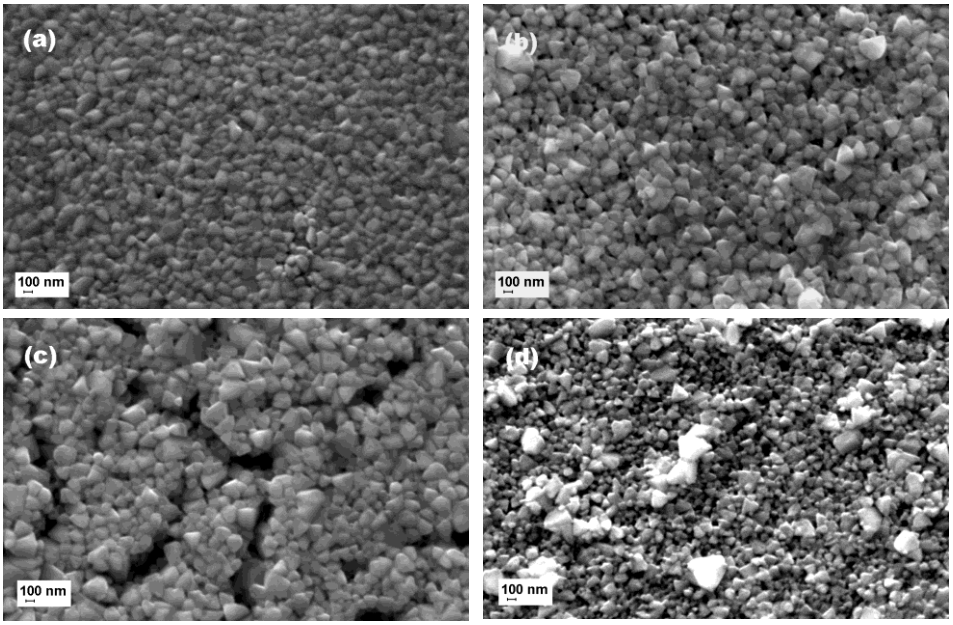

Figure 3

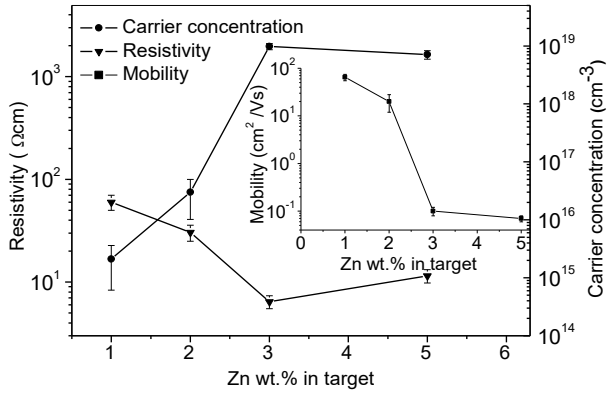

Figure 4

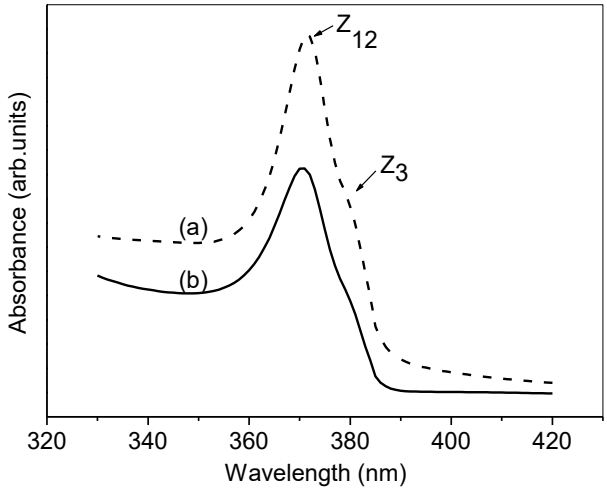

Figure 5

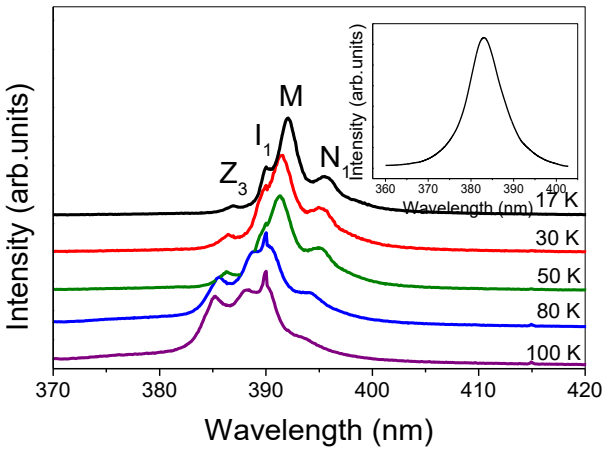
Intensity (arb.units)
Wavelength (nm)
370
380
390
400
410
420
Z3
I1
M
N1
17 K
30 K
50 K
80 K
100 K
Intensity (arb.units)
Wavelength (nm)
360
370
380
390
400

Figure 6